35th Annual International Conference of the IEEE EMBS
Osaka, Japan, 3 - 7 July, 2013

# Experiment-Based Scatter Correction for Cone-Beam Computed Tomography Using the Statistical Method

Sorapong Aootaphao, Saowapak S.Thongvigitmanee, Jatuwat Rajruangrabin, Parinya Junhunee, and Pairash Thajchayapong

*Abstract*— **Scatter signals in cone-beam computed tomography (CBCT) cause a significant problem that degrades image quality of reconstructed images, such as inaccuracy of CT numbers and cupping artifacts. In this paper, we will present an experiment-based scatter correction method by pre-processing projection images using a statistical model combined with experimental kernels. The convolution kernels are estimated by using different thickness of PMMA plates attached to a beam stop lead sheet such that the scatter signal values can be measure in the shadow area of the projection images caused by the lead sheet. The scatter signal values of different thickness levels can be measured in the shadow area of projection images caused by the lead sheet. Then, the projection images are convolved with the kernels that are derived from the actual measurement of scatter signals in PMMA plates. Finally, the primary signals can be estimated using the maximum likelihood expectation maximization method. Experimental results by using the proposed method show that the quality of the reconstruction images is significantly improved. The CT numbers become more accurate and the cupping artifact is reduced.**

## I. Introduction

Cone-beam computed tomography (CBCT) imaging systems with flat panel detectors have attracted more interest in dental and maxillofacial imaging in the recent years due to their accurate 3D information and minimal radiation dose. Commonly, scatter signal values in small area detectors are smaller than those of large area detectors. Thus, medical CT scanners have small values of scatter to primary ratio (SPR), unlike CBCT scanners where SPR values are more than 1 [1]. It is well known that image quality in cross-sectional images is degraded by X-ray scatter signals, yielding incorrect CT numbers and cupping artifacts. However, the quantity of X-ray scatter signals depends on various factors, such as the field of view (FOV), the object size, and X-ray beam energy.

Although many scatter correction methods have been published, there exist two main scatter correction methods [2]-[6]. The first method is the physical removal of scatter signals before detection which is mostly used in medical CT scanners, such as anti-scatter grids, air gaps and slit devices [2]. The second method is numerical compensation, such as convolution-subtraction techniques [3], [4] and deconvolution by Fourier transforms [5], [6]. The convolution-subtraction technique may produce the negative primary values which are not theoretically correct [7].

In this paper, we propose the experiment-based scatter correction method. We apply the maximum likelihood expectation maximization (MLEM) [8], [9] method and experimental kernels to obtain primary signal values. In addition, the experimental results will be benchmarked with fan beam computed tomography (FBCT) in similar CT system settings. The remainder of this paper is organized as follows. First, we will describe scatter modeling and the overall concept of the proposed scatter correction steps. The next section will explain how to construct the kernels from measurement data. Then, we describe the thickness mapping method with projection images. The experimental results before and after scatter correction are compared with FBCT. The final section will be the conclusion and future work.

## II. Scatter Modeling and Overall concept

Our CBCT system consists of the flat panel detector (Varian PaxScan 2520D) with the pixel size of 0.254 mm, and the X-ray source with 90 kVp. A full rotation of scan with an increment of 1 degree is achieved to acquire 360 projection images. Those images will be corrected before reconstruction. Normally, the measured signal ($I_m$) in the projection images contains both primary and scatter signals, so $I_m$ can be written as:

$$I_m(x,y) = I_p(x,y) + I_s(x,y) \tag{1}$$

where $I_p$ is the primary signal which is what we desire, $I_s$ is the scatter signal which can be measured, $x$ and $y$ denote pixel coordinates in a projection image. The scatter signal can be written in the form of the primary signal convolved with the kernel function, $K$, as follows:

$$I_s(x,y) = I_p(x,y) ** K(x,y) \tag{2}$$

where ** denotes a 2-D convolution operator. To estimate the primary signal, we use the iterative MLEM algorithm as follows:

This work is supported by the National Science and Technology Development Agency, Thailand.

Sorapong Aootaphao, Saowapak S. Thongvigitmanee, and Jatuwat Rajruangrabin are with the Image Technology Lab, Intelligent Informatics Research Unit, National Electronics and Computer Technology Center, Thailand (corresponding author; phone: 662-564-6900; fax: 662-564-6873; e-mail: sorapong.aootaphao@nectec.or.th).

Parinya Junhunee is with the Medical Devices Lab, Biomedical Engineering Research Unit, National Metal and Materials Technology Center, Thailand.

Pairash Thajchayapong is with the National Science and Technology Development Agency, Pathumthani, Thailand.

$$I_p^{q+1}(x,y) = \frac{I_p^q(x,y) \times I_m(x,y)}{I_p^q(x,y) + I_p^q(x,y) ** K(x,y)} \quad (3)$$

where $I_p^q$ is the primary signal estimated at the $q^{th}$ iteration. The scatter correction process starts by creating a database of kernels according to thickness of PMMA plates [10], and initializing the primary signal $I_p^0(x,y)$. The next step is to match each pixel of the primary signal with estimated PMMA equivalent thicknesses, i.e., the data are divided into different groups according to thickness. The sub-data sets of the primary signal are convolved with the kernels and summed up. And then, the summed result is used to perform deconvolution by the MLEM algorithm. Finally, we check the condition for convergence. If it does not converge, we will return to the thickness mapping process again. In summary, all steps of the scatter correction can be illustrated as follows in Fig. 1.

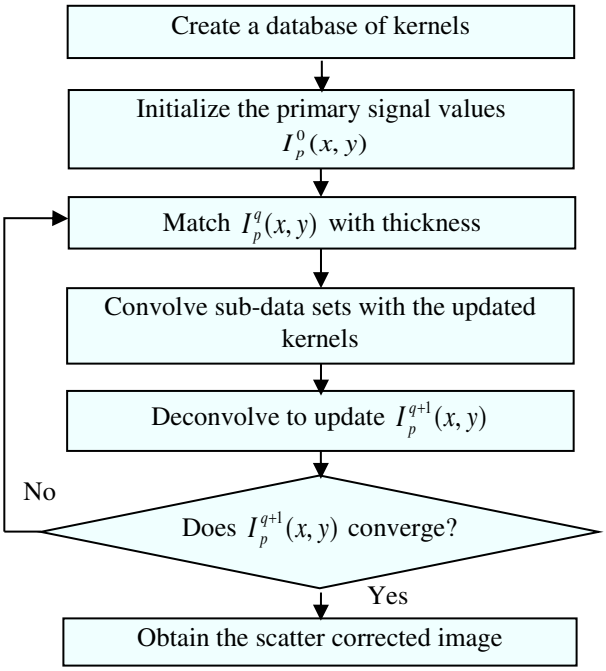


Figure 1. The overall scatter correction process

## III. Kernel Measurements

The calculation of kernels is one of the key factors for successful deconvolution. The spreading distances and amplitudes of the scatter signal depend on thickness of the object, which can be described as follows:

$$K_t(x,y) = A(t) \times h_t(x,y) \quad (4)$$

where $A(t)$ is the amplitude term which is derived from the scatter fraction (SF) at each thickness, $h_t(x,y)$ is the exponential term that forms the shape of the kernel, $t$ is thickness values. Thus, the kernel measurements consist of two parts to consider: the $h_t$ term and the amplitude term. In the first part, we measure the kernel shape from the scatter signal in the projection images. For the experimental setup of kernel shape measurement, we used the total of 14 sets, as one set of the PMMA plates is 9 mm. Thus, the total length of the PMMA plates in the experiment is 126 mm. The lead sheet is placed on top of the PMMA plates, while the edge region of the PMMA with the lead sheet aligns with the beam center of X-ray. Hence, the scatter signal can be measured through a profile in a projection image at the shadow of a lead sheet with different PMMA thickness as shown in Fig. 2 a). In our experiments, to achieve the thickness map at 1 mm, the projection data sets of PMMA plates at each thickness are interpolated. Thus, the $h_t$ term is calculated at each thickness of 1 mm as shown in Fig. 2 b). In the second part, the amplitude term to form the kernel is the SF function. This SF function can be derived by measuring the amplitude of the scatter signal near the edge of the lead sheet for different PMMA thickness. The plot of the SF function versus the thickness is shown in Fig. 3.

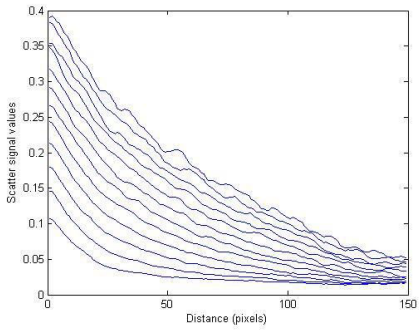


a)

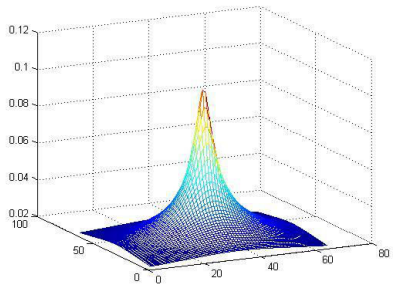

b)

Figure 2. a) Profiles of scatter signal values at each thickness, b) The normalized kernel calculated from LSF.

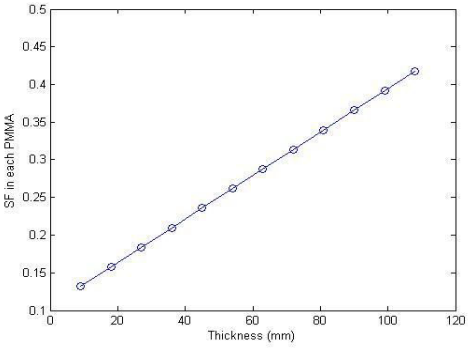


Figure 3. The scatter fraction versus thickness

## IV. Thickness Map Measurements

To construct the thickness map, first, we create the log signal function at each thickness of pure PMMA plates [3], [4], [10]. One set of PMMA plates has the thickness of 9 mm and the total of 14 sets is used in this work. To compute the PMMA equivalent thickness, $t$, we derive the Beer's law [11] as follows:

$$t = \frac{1}{\mu_{PMMA}} \log\left(\frac{I_{m,0}}{I_m}\right) \tag{5}$$

where $\mu_{PMMA}$ is the linear attenuation coefficient of PMMA materials, $I_{m,0}$, is the measured signal of a blank scan and $I_m$ is the measured signal of an object. Fig. 4 shows the derived log signal plot in terms of thickness. Since the ideal plot between the log signal term and thickness is linear, we employ linear curve fitting to the real data.

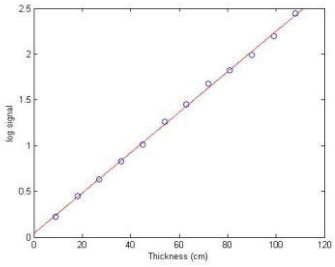


Figure 4. The log signal versus thickness

## V. Experimental Results

To illustrate the performance of the proposed technique, we tested with 2 objects: the PMMA plate with the lead sheet and our own design phantom. In our experiment, we divided the projection data of an object into 15 groups, where each size of a group is 8 mm. Fig. 5 shows a few examples of sub-data sets after grouping their thickness through different intensities of projections. Fig. 6 shows the profiles of the scatter corrected results in the first object, where the blue dashed line is the scatter corrected signal, and the red solid line is the original measured signal. In the second object, our own design phantom consists of various materials: Teflon, Delrin, PMMA, Nylon, Water and Air. Fig. 7 shows the profiles of the estimated primary signal and the measured signal in the phantom image. As expected, the $I_p$ values (blue dashed line) are smaller than the $I_m$ values (red solid line). Although the estimated primary signal values after scatter correction contained high frequency noise, we ignored noise suppression in this study. Once the data sets of projection images were corrected, we reconstructed cross-sectional images by filtered backprojection (FBP) reconstruction [10]. For this study, we used the Hamming filter with the cutoff of 0.85 to obtain good quality of reconstructed images. Fig. 8 a) and b) show the comparison of the reconstructed images before and after scatter correction, respectively. Fig. 8 c) compares the results through the profiles. It is noticed that the cupping artifact of the scatter corrected profiles is reduced and the contrasts in the inserts are increased. For quantitative analysis, the results of scatter correction in CT number values are benchmarked with FBCT as shown in Table I. After scatter correction, the CT numbers of all materials in CBCT are approaching those in the FBCT system. Table II shows the comparison of noise (standard deviation) with and without scatter correction. This confirms that noise is increased after scatter correction, which agrees with the FBCT system.

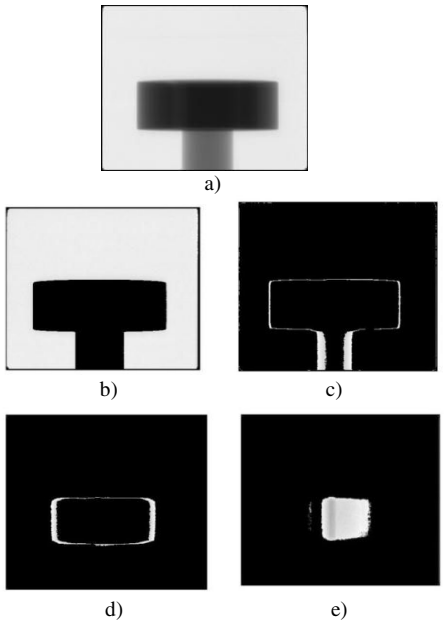


Figure 5. a) Measured projection image, b)-e) sub-data sets after matching the thickness map at 0, 50,80, 100 mm

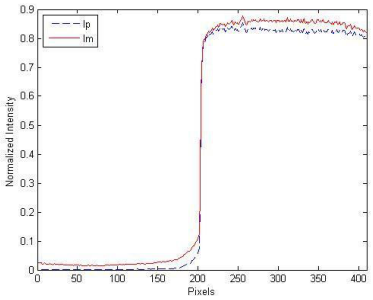


Figure 6. Comparison of intensity profiles in the projection image of the PMMA with the lead sheet before and after scatter correction

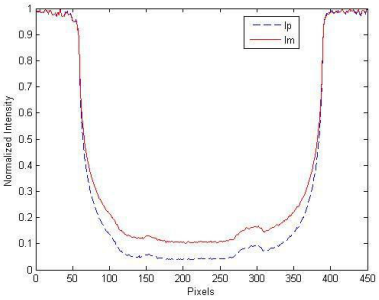


Figure 7. Comparison of intensity profiles in the phantom image before and after scatter correction

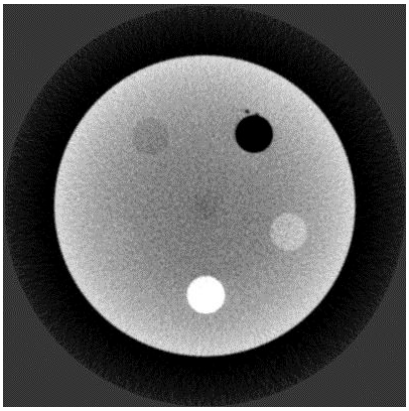

a)

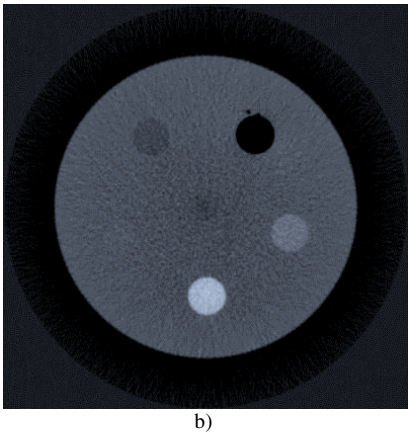

b)

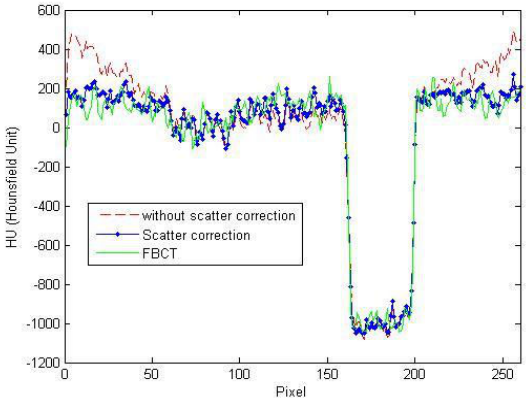


c)

Figure 8. Comparison of the scatter corrected results a) without scatter correction, b) with scatter correction, c) profile results

TABLE I. COMPARISON OF CT NUMBER VALUES AND ABSOLUTE ERRORS IN PERCENTAGE

| | **FBCT** | **CBCT No Correction** | | **CBCT Scatter Correction** | |
|---|---|---|---|---|---|
| | HU | HU | % Error | HU | % Error |
| Teflon | 917 | 860 | 6.2 | 924 | 0.76 |
| Delrin | 334 | 308 | 7.78 | 339 | 1.49 |
| PMMA | 121 | 118 | 2.47 | 125 | 3.3 |
| Nylon | 97.3 | 90 | 7.5 | 101 | 1.64 |

TABLE II. COMPARISON OF NOISE VALUES (STANDARD DEVIATION)

| | **FBCT** | **CBCT without scatter correction** | **CBCT with scatter correction** |
|---|---|---|---|
| Teflon | 94 | 56.7 | 90 |
| Delrin | 88 | 48 | 78 |
| PMMA | 74 | 37 | 69 |
| Nylon | 78 | 41 | 73 |

## VI. CONCLUSION

The scatter correction method in cone-beam computed tomography is proposed in this paper. Our proposed methods start with the measurement kernels derived from the experimental results and find the PMMA equivalent thickness map in the projection images. Then, the primary signal projection images are estimated by the MLEM method. The quality of reconstructed images after scatter correction is improved in terms of higher CT number accuracy and smaller cupping artifacts in comparison with the results obtained from FBCT. The pitfall of scatter correction is an increase in high frequency noise in the reconstruction images as the number of iterations is increased. For future work, we will work on reducing such high frequency noise in the projection images.

## REFERENCES


[1] Y. Kyriakou, and W. A. Kalender, "X-ray scatter data for flat-panel detector CT," *Med Phys*, vol. 23, pp. 3-15, March 2007.

[2] J. Persliden, and G. A. Carlsson, "Scatter rejection by air gaps in diagnostic radiology calculations using a monte carlo collision density method and consideration of molecular interference in coherent scattering," *Med Phys*, vol. 42, pp. 155-75, 1997.

[3] J. Star-Lack, M. Sun, A. Kaestner, and R. Hassanein, "Efficient scatter correction using asymmetric kernels," *Proc. of SPIE*, vol. 7258, pp. 72581Z1-12, 2009.

[4] I. Reitz, B.-M. Hesse, S. Nill, T. Tucking, and U. Oelfke, "Enhancement of image quality with a fast iterative scatter and beam hardening correction method for kV CBCT," *Med Phys,* vol.19, pp. 158-172, March 2009.

[5] J. L. Ducote, and S. Molloi, "Scatter correction in digital mammography based on image deconvolution," *Med Phys*, vol. 55, pp. 1295-1309, 2010.

[6] J. A. Seibert, and J. M. Boone, "X-ray scatter removal by deconvolution," *Med. Phys*, vol. 15, pp. 567-576, 1988.

[7] J. S. Maltz, B. Gangadharan, S. Bose, D. H. Hristov, B. A. Faddegon, A. Paidi, and A. R. Bani-Hashemi, "Algorithm for X-ray Scatter, Beam-Hardening, and Beam Profile Correction in Diagnostic (Kilovoltage) and Treatment (Megavoltage) Cone Beam CT," *IEEE Trans.* Medical Imaging, vol. 27, no. 12, pp 1791-1810, December 2008.

[8] A. H. Baydush, and C. E. Floyd, "Jr. Bayesian image estimation of digital chest radiography: Interdependence of noise, resolution, and scatter fraction," *Med Phys*, vol. 22(8), pp. 1255-1216, 1995.

[9] H. Li, R. Mohan, and X. R. Zhu, "Derivation of Scatter Kernel in CBCT Imaging System," *Signals, Systems and Computer*, pp. 1851 - 1854, Oct. 29-Nov. 1 2006.

[10] S. K. Ahn, G. Cho, and H. Jeon, "A Scatter Correction Using Thickness Iteration in Dual-Energy Radiography," *IEEE Trans.* Nuclear Science, vol. 53, no. 1, February 2006.

[11] A. C. Kak, and M. Slaney, "Principles of Computerized Tomographic Imaging," *IEEE Press*, NY, 1988.